Monthly Notices
of the
ROYAL ASTRONOMICAL SOCIETY

Mon. Not. R. Astron. Soc. **426,** 739–750 (2012) doi:10.1111/j.1365-2966.2012.21780.x

Seven transiting hot Jupiters from WASP-South, Euler and TRAPPIST: WASP-47b, WASP-55b, WASP-61b, WASP-62b, WASP-63b, WASP-66b and WASP-67b

Coel Hellier,[1⋆] D. R. Anderson,[1] A. Collier Cameron,[2] A. P. Doyle,[1] A. Fumel,[3] M. Gillon,[3] E. Jehin,[3] M. Lendl,[4] P. F. L. Maxted,[1] F. Pepe,[4] D. Pollacco,[5] D. Queloz,[4] D. Ségransan,[4] B. Smalley,[1] A. M. S. Smith,[1] J. Southworth,[1] A. H. M. J. Triaud,[4] S. Udry[4] and R. G. West[6]

[1]*Astrophysics Group, Keele University, Staffordshire ST5 5BG*
[2]*SUPA, School of Physics and Astronomy, University of St. Andrews, North Haugh, Fife KY16 9SS*
[3]*Institut d'Astrophysique et de Géophysique, Université de Liège, Allée du 6 Août 17, Bat. B5C, Liège 1, Belgium*
[4]*Observatoire astronomique de l'Université de Genève, 51 ch. des Maillettes, 1290 Sauverny, Switzerland*
[5]*Astrophysics Research Centre, School of Mathematics & Physics, Queen's University, University Road, Belfast BT7 1NN*
[6]*Department of Physics and Astronomy, University of Leicester, Leicester LE1 7RH*

Accepted 2012 July 23. Received 2012 July 23; in original form 2012 April 23

ABSTRACT

We present seven new transiting hot Jupiters from the WASP-South survey. The planets are all typical hot Jupiters orbiting stars from F4 to K0 with magnitudes of $V = 10.3$–12.5. The orbital periods are all in the range of 3.9–4.6 d, the planetary masses range from 0.4 to 2.3 $M_{\rm Jup}$ and the radii from 1.1 to 1.4 $R_{\rm Jup}$. In line with known hot Jupiters, the planetary densities range from Jupiter-like to inflated ($\rho = 0.13$–$1.07\rho_{\rm Jup}$). We use the increasing numbers of known hot Jupiters to investigate the distribution of their orbital periods and the 3–4 d 'pile-up'.

Key words: planetary systems.

1 INTRODUCTION

Transiting exoplanets found by the ground-based transit searches are mostly 'hot Jupiters', Jupiter-sized planets in ≈1–6 d orbits, since these are the easiest planets for such surveys to find. However, planet candidate lists from *Kepler* show that hot Jupiters are much less common than smaller planets (Batalha et al. 2012). This means that the much larger sky coverage of the ground-based surveys (e.g. HATnet, Bakos et al. 2004; WASP, Pollacco et al. 2006) is needed to produce large samples of hot Jupiters that will enable us to understand the properties of this class. In addition, hot Jupiters from these surveys orbit stars of $V \approx 9$–13, which are bright enough for radial-velocity measurements of the planetary masses and for many other types of study.

Here we present seven new transiting planets discovered by the WASP-South survey (Hellier et al. 2011a) in conjunction with the Euler/CORALIE spectrograph and the TRAPPIST robotic photometer (Jehin et al. 2011). These are all hot Jupiters with ∼4 d orbits that are compatible with being circular, and with masses and radii that are typical of the class. They all orbit relatively isolated stars of $V = 10.3$–12.5 which have metallicities and space velocities compatible with local thin-disc stars. WASP-South planets that are less typical of the class will be reported in other papers.

2 OBSERVATIONS

WASP-South uses an eight-camera array that covers 450 deg^2 of sky observing with a typical cadence of 8 min. The WASP surveys are described in Pollacco et al. (2006) while a discussion of our planet-hunting methods can be found in Collier Cameron et al. (2007a) and Pollacco et al. (2008).

WASP-South planet candidates are followed up using the TRAPPIST robotic photometer and the CORALIE spectrograph on the Euler 1.2-m telescope at La Silla. About one in 12 candidates turns out to be a planet, the remainder being blends that are unresolved in the WASP data (which uses 14 arcsec pixel) or astrophysical transit mimics, usually eclipsing binary stars. A list of observations reported in this paper is given in Table 1, while the CORALIE radial velocities are listed in Table A1 (with the online version of the paper – see Supporting Information).

3 THE HOST STARS

The CORALIE spectra of the host stars were co-added to produce spectra for analysis using the methods described in Gillon

⋆E-mail: ch@astro.keele.ac.uk

Table 1. Observations.

Facility	Date	
WASP-47		
WASP-South	2008 June–2010 October	18 300 points
Euler/CORALIE	2010 May–2011 November	19 radial velocities
EulerCAM	2011 August 2	Gunn r filter
WASP-55		
WASP-South	2006 May–2010 July	28 200 points
Euler/CORALIE	2011 January–2011 July	20 radial velocities
TRAPPIST	2011 April 4	$I+z$ filter
EulerCAM	2011 June 3	Gunn r filter
TRAPPIST	2012 January 20	$I+z$ filter
WASP-61		
WASP-South	2006 September–2010 February	30 700 points
Euler/CORALIE	2011 January–2011 November	15 radial velocities
TRAPPIST	2011 September 9	Blue-block filter
EulerCAM	2011 November 16	Gunn r filter
TRAPPIST	2011 November 16	Blue-block filter
TRAPPIST	2011 December 9	Blue-block filter
TRAPPIST	2011 December 13	Blue-block filter
WASP-62		
WASP-South	2008 September–2011 February	21 700 points
Euler/CORALIE	2011 March–2012 April	25 radial velocities
EulerCAM	2011 November 24	Gunn r filter
TRAPPIST	2011 December 17	z-band filter
WASP-63		
WASP-South	2006 October–2010 March	24 700 points
Euler/CORALIE	2011 February–2012 April	23 radial velocities
TRAPPIST	2011 December 4	z-band filter
EulerCAM	2011 December 25	Gunn r filter
EulerCAM	2012 January 29	Gunn r filter
TRAPPIST	2012 February 21	$I+z$ filter
WASP-66		
WASP-South	2006 May–2011 June	19 600 points
Euler/CORALIE	2011 January–2012 March	30 radial velocities
TRAPPIST	2011 April 8	$I+z$ filter
TRAPPIST	2011 December 21	$I+z$ filter
TRAPPIST	2012 March 16	Blue-block filter
EulerCAM	2012 March 16	Gunn r filter
WASP-67		
WASP-South	2006 May–2010 September	12 500 points
Euler/CORALIE	2011 July–2011 October	19 radial velocities
TRAPPIST	2011 September 29	$I+z$ filter
EulerCAM	2011 September 29	Gunn r filter

Table 2. System parameters for WASP-47.

1SWASP J220448.72−120107.8	
2MASS 22044873−1201079	
RA = $22^{\rm h}04^{\rm m}48\overset{\rm s}{.}72$, Dec, = $-12^\circ01'07\overset{''}{.}8$ (J2000)	
V mag = 11.9	
Rotational modulation	<0.7 mmag (95 per cent)
pm (RA) 17.1 ± 1.1 (Dec.) –42.9 ± 1.0 mas yr^{-1}	
Stellar parameters from spectroscopic analysis.	
Spectral type	G9V
$T_{\rm eff}$ (K)	5400 ± 100
log g	4.55 ± 0.10
$\xi_{\rm t}$ (km s^{-1})	0.7 ± 0.2
$v \sin I$ (km s^{-1})	3.0 ± 0.6
[Fe/H]	0.18 ± 0.07
[Na/H]	0.42 ± 0.06
[Mg/H]	0.21 ± 0.04
[Si/H]	0.36 ± 0.07
[Ca/H]	0.15 ± 0.11
[Ti/H]	0.28 ± 0.06
[Cr/H]	0.21 ± 0.10
[Ni/H]	0.30 ± 0.09
log A(Li)	<0.81 ± 0.10
Distance	200 ± 30 pc
Parameters from MCMC analysis.	
P (d)	4.159 1399 ± 0.000 0072
$T_{\rm c}$ (HJD) (UTC)	245 5764.346 02 ± 0.000 22
T_{14} (d)	0.149 33 ± 0.000 65
$T_{12} = T_{34}$ (d)	$0.0141^{+0.0007}_{-0.0003}$
$\Delta F = R_{\rm P}^2/R_*^2$	0.010 51 ± 0.000 14
b	0.14 ± 0.11
i (°)	$89.2^{+0.5}_{-0.7}$
K_1 (km s^{-1})	0.136 ± 0.005
γ (km s^{-1})	–27.056 ± 0.004
e	0 (adopted) (<0.11 at 3σ)
M_* ($M_\odot$)	1.084 ± 0.037
R_* ($R_\odot$)	$1.15^{+0.03}_{-0.02}$
log g_* (CGS)	$4.348^{+0.009}_{-0.016}$
ρ_* ($\rho_\odot$)	$0.71^{+0.02}_{-0.04}$
$T_{\rm eff}$ (K)	5350 ± 90
$M_{\rm P}$ ($M_{\rm Jup}$)	1.14 ± 0.05
$R_{\rm P}$ ($R_{\rm Jup}$)	$1.15^{+0.04}_{-0.02}$
log $g_{\rm P}$ (CGS)	$3.29^{+0.02}_{-0.03}$
$\rho_{\rm P}$ ($\rho_{\rm J}$)	$0.74^{+0.05}_{-0.06}$
$\rho_{\rm P}$ (CGS)	$0.99^{+0.06}_{-0.08}$
a (au)	0.0520 ± 0.0006
$T_{\rm P,A\,=0}$ (K)	1220 ± 20

Errors are 1σ; Limb-darkening coefficients were (Euler r) a1 = 0.727, a2 = −0.653, a3 = 1.314 and a4 = −0.594.

et al. (2009). We used the Hα line to determine the effective temperature ($T_{\rm eff}$), and the Na I D and Mg I b lines as diagnostics of the surface gravity ($\log g_*$). The resulting parameters are listed in Tables 2–8. The elemental abundances were determined from equivalent-width measurements of several clean and unblended lines. A value for microturbulence ($\xi_{\rm t}$) was determined from Fe I lines using the criteria of a null dependence of line abundances with equivalent width (see Magain 1984). The quoted error estimates include that given by the uncertainties in $T_{\rm eff}$, $\log g_*$ and $\xi_{\rm t}$, as well as the scatter due to measurement and atomic data uncertainties.

The projected stellar rotation velocities ($v \sin I$) were determined by fitting the profiles of several unblended Fe I lines. We used values for macroturbulence ($v_{\rm mac}$) from the tabulation by Bruntt et al. (2010). A CORALIE instrumental full width at half-maximum of 0.11 ± 0.01 Å was determined from the telluric lines around 6300 Å.

3.1 Rotational modulation

We searched the WASP photometry of each star for rotational modulations by using a sine-wave fitting algorithm as described by Maxted et al. (2011). We estimated the significance of periodicities by subtracting the fitted transit light curve and then repeatedly and randomly permuting the nights of observation. For none of our stars was a significant periodicity obtained, with 95 per cent confidence upper limits being typically 1 mmag (as listed in Tables 2–8).

3.2 Proper motions

For each of our stars we list (Tables 2–8) the proper motions from the UCAC3 catalogue (Zacharias et al. 2010). Combining these with the spectroscopic distances and the radial velocities in the same tables

Table 3. System parameters for WASP-55.

1SWASP J133501.94−173012.7	
2MASS 13350194−1730124	
TYCHO-2 6125-113-1	
RA = $13^h35^m01^s.94$, Dec. = $-17°30'12''.7$ (J2000)	
V mag = 11.8	
Rotational modulation	<1 mmag (95 per cent)
pm (RA) 11.2 ± 1.0 (Dec.) -8.2 ± 1.0 mas yr^{-1}	
Stellar parameters from spectroscopic analysis.	
Spectral type	G1
$T_{\rm eff}$ (K)	5900 ± 100
$\log g$	4.3 ± 0.1
$\xi_{\rm t}$ (km s^{-1})	1.1 ± 0.1
$v \sin I$ (km s^{-1})	3.1 ± 1.0
[Fe/H]	-0.20 ± 0.08
[Na/H]	-0.21 ± 0.05
[Mg/H]	-0.17 ± 0.04
[Si/H]	-0.13 ± 0.05
[Ca/H]	-0.10 ± 0.10
[Sc/H]	-0.05 ± 0.08
[Ti/H]	-0.08 ± 0.05
[Cr/H]	-0.18 ± 0.07
[Ni/H]	-0.21 ± 0.06
$\log A$(Li)	2.36 ± 0.09
Distance	330 ± 50 pc
Parameters from MCMC analysis.	
P (d)	$4.465\,633 \pm 0.000\,004$
$T_{\rm c}$ (HJD) (UTC)	$245\,5737.9396 \pm 0.0003$
T_{14} (d)	0.147 ± 0.001
$T_{12} = T_{34}$ (d)	$0.0167^{+0.0011}_{-0.0004}$
$\Delta F = R_{\rm P}^2/R_*^2$	0.0158 ± 0.0003
b	0.15 ± 0.12
i (°)	89.2 ± 0.6
K_1 (km s^{-1})	0.070 ± 0.004
γ (km s^{-1})	-4.3244 ± 0.0009
e	0 (adopted) (<0.20 at 3σ)
M_* ($M_\odot$)	1.01 ± 0.04
R_* ($R_\odot$)	$1.06^{+0.03}_{-0.02}$
$\log g_*$ (CGS)	$4.39^{+0.01}_{-0.02}$
ρ_* ($\rho_\odot$)	$0.85^{+0.03}_{-0.07}$
$T_{\rm eff}$ (K)	5960 ± 100
$M_{\rm P}$ ($M_{\rm Jup}$)	0.57 ± 0.04
$R_{\rm P}$ ($R_{\rm Jup}$)	$1.30^{+0.05}_{-0.03}$
$\log g_{\rm P}$ (CGS)	2.89 ± 0.04
$\rho_{\rm P}$ ($\rho_{\rm J}$)	$0.26^{+0.02}_{-0.03}$
$\rho_{\rm P}$ (CGS)	$0.34^{+0.03}_{-0.04}$
a (au)	0.0533 ± 0.0007
$T_{\rm P,A\,=0}$ (K)	1290 ± 25

Errors are 1σ; Limb-darkening coefficients were (Euler r) a1 = 0.496, a2 = 0.201, a3 = 0.183 and a4 = −0.170; (Trapp Iz) a1 = 0.587, a2 = −0.180, a3 = 0.441 and a4 = −0.250.

Table 4. System parameters for WASP-61.

1SWASP J050111.91−260314.9	
2MASS 05011191−2603149	
TYCHO-2 6469-1972-1	
RA = $05^h01^m11^s.91$, Dec. = $-26°03'14''.9$ (J2000)	
V mag = 12.5	
Rotational modulation	<1.5 mmag (95 per cent)
pm (RA) 1.0 ± 0.9 (Dec.) 0.5 ± 1.0 mas yr^{-1}	
Stellar parameters from spectroscopic analysis.	
Spectral type	F7
$T_{\rm eff}$ (K)	6250 ± 150
$\log g$	4.3 ± 0.1
$\xi_{\rm t}$ (km s^{-1})	1.0 ± 0.2
$v \sin I$ (km s^{-1})	10.3 ± 0.5
[Fe/H]	-0.10 ± 0.12
$\log A$(Li)	$<1.13 \pm 0.11$
Distance	480 ± 65 pc
Parameters from MCMC analysis.	
P (d)	$3.855\,900 \pm 0.000\,003$
$T_{\rm c}$ (HJD) (UTC)	$245\,5859.528\,25 \pm 0.000\,23$
T_{14} (d)	0.1642 ± 0.0006
$T_{12} = T_{34}$ (d)	$0.0142^{+0.0004}_{-0.0002}$
$\Delta F = R_{\rm P}^2/R_*^2$	0.0088 ± 0.0001
b	$0.09^{+0.09}_{-0.06}$
i (°)	$89.35^{+0.45}_{-0.66}$
K_1 (km s^{-1})	0.233 ± 0.016
γ (km s^{-1})	18.970 ± 0.002
e	0 (adopted) (<0.26 at 3σ)
M_* ($M_\odot$)	1.22 ± 0.07
R_* ($R_\odot$)	1.36 ± 0.03
$\log g_*$ (CGS)	4.256 ± 0.011
ρ_* ($\rho_\odot$)	$0.487^{+0.008}_{-0.017}$
$T_{\rm eff}$ (K)	6320 ± 140
$M_{\rm P}$ ($M_{\rm Jup}$)	2.06 ± 0.17
$R_{\rm P}$ ($R_{\rm Jup}$)	1.24 ± 0.03
$\log g_{\rm P}$ (CGS)	3.48 ± 0.03
$\rho_{\rm P}$ ($\rho_{\rm J}$)	1.07 ± 0.09
$\rho_{\rm P}$ (CGS)	1.42 ± 0.12
a (au)	0.0514 ± 0.0009
$T_{\rm P,A\,=0}$ (K)	1565 ± 35

Errors are 1σ; Limb-darkening coefficients were (All) a1 = 0.466, a2 = 0.414, a3 = −0.192 and a4 = 0.002.

gives space velocities in the range of 19–55 km s^{-1}. Our stars are all compatible with the local thin-disc population, which typically has $-0.6 <$ [Fe/H] < 0.3 and $\sigma_{\rm v} \approx 50$ km s^{-1} (Navarro et al. 2011).

4 SYSTEM PARAMETERS

The CORALIE radial-velocity measurements were combined with the WASP, EulerCAM and TRAPPIST photometry in a simultaneous Markov chain Monte Carlo (MCMC) analysis to find the system parameters. For details of our methods see Collier Cameron et al. (2007b). The limb-darkening parameters are noted in each table, and are taken from the four-parameter non-linear law of Claret (2000).

For all of our planets the data are compatible with zero eccentricity and hence we imposed a circular orbit (see Anderson et al. 2012 for a discussion of the rationale for this). The fitted parameters were thus $T_{\rm c}$, P, ΔF, T_{14}, b and K_1, where $T_{\rm c}$ is the epoch of mid-transit, P is the orbital period, ΔF is the fractional flux deficit that would be observed during transit in the absence of limb darkening, T_{14} is the total transit duration (from first to fourth contact), b is the impact parameter of the planet's path across the stellar disc and K_1 is the stellar reflex velocity semi-amplitude.

The transit light curves lead directly to stellar density but one additional constraint is required to obtain stellar masses and radii, and hence full parametrization of the system. We adopt the approach of Enoch et al. (2010), based on empirical calibrations of stellar properties from well-studied detached eclipsing binary systems, but we use the calibration coefficients calculated by Southworth (2011). These are improvements on the coefficients from Enoch et al. as they include far more stars (180 versus 38) and also restrict the calibration sample to objects with masses relevant to the study

Table 5. System parameters for WASP-62.

1SWASP J054833.59−635918.3	
2MASS 05483359−6359183	
TYCHO-2 8900-874-1	
RA = 05^{h}48^{m}33^s.59, Dec. = −63°59′18″.3 (J2000)	
V mag = 10.3	
Rotational modulation	<1 mmag (95 per cent)
pm (RA) −14.0 ± 0.9 (Dec.) −27.0 ± 1.0 mas yr^{-1}	
Stellar parameters from spectroscopic analysis.	
Spectral type	F7
$T_{\rm eff}$ (K)	6230 ± 80
log g	4.45 ± 0.10
$\xi_{\rm t}$ (km s^{-1})	1.25 ± 0.10
$v \sin I$ (km s^{-1})	8.7 ± 0.4
[Fe/H]	0.04 ± 0.06
[Na/H]	−0.02 ± 0.03
[Mg/H]	0.07 ± 0.08
[Al/H]	0.03 ± 0.03
[Si/H]	0.11 ± 0.08
[Ca/H]	0.16 ± 0.12
[Sc/H]	0.10 ± 0.05
[Ti/H]	0.11 ± 0.08
[V/H]	0.01 ± 0.09
[Cr/H]	0.09 ± 0.07
[Mn/H]	−0.08 ± 0.05
[Co/H]	−0.02 ± 0.10
[Ni/H]	0.04 ± 0.08
log A(Li)	2.48 ± 0.06
Distance	160 ± 30 pc
Parameters from MCMC analysis.	
P (d)	4.411 953 ± 0.000 003
$T_{\rm c}$ (HJD) (UTC)	245 5855.391 95 ± 0.000 27
T_{14} (d)	0.1588 ± 0.0014
$T_{12} = T_{34}$ (d)	0.0172 ± 0.0012
$\Delta F = R_{\rm P}^2/R_*^2$	0.0123 ± 0.0002
b	$0.29^{+0.08}_{-0.14}$
i (°)	$88.3^{+0.9}_{-0.6}$
K_1 (km s^{-1})	0.060 ± 0.004
γ (km s^{-1})	14.970 ± 0.005
e	0 (adopted) (<0.21 at 3σ)
M_* ($M_\odot$)	1.25 ± 0.05
R_* ($R_\odot$)	1.28 ± 0.05
log g_* (CGS)	4.316 ± 0.025
ρ_* ($\rho_\odot$)	0.59 ± 0.06
$T_{\rm eff}$ (K)	6280 ± 80
$M_{\rm P}$ ($M_{\rm Jup}$)	0.57 ± 0.04
$R_{\rm P}$ ($R_{\rm Jup}$)	1.39 ± 0.06
log $g_{\rm P}$ (CGS)	2.83 ± 0.04
$\rho_{\rm P}$ ($\rho_{\rm J}$)	0.21 ± 0.03
$\rho_{\rm P}$ (CGS)	0.28 ± 0.04
a (au)	0.0567 ± 0.0007
$T_{\rm P,A\,=0}$ (K)	1440 ± 30

Errors are 1σ; Limb-darkening coefficients were (Euler r) a1 = 0.508, a2 = 0.269, a3 = 0.015 and a4 = −0.090; (Trapp Iz) a1 = 0.585, a2 = −0.095, a3 = 0.276 and a4 = −0.176.

Table 6. System parameters for WASP-63.

1SWASP J061720.74−381923.8	
2MASS 06172074−3819237	
TYCHO-2 7612-556-1	
RA = 06^{h}17^{m}20^s.74, Dec. = −38°19′23″.8 (J2000)	
V mag = 11.2	
Rotational modulation	<0.8 mmag (95 per cent)
pm (RA) −16.5 ± 0.9 (Dec.) −26.7 ± 0.9 mas yr^{-1}	
Stellar parameters from spectroscopic analysis.	
Spectral type	G8
$T_{\rm eff}$ (K)	5550 ± 100
log g	3.9 ± 0.1
$\xi_{\rm t}$ (km s^{-1})	0.9 ± 0.1
$v \sin I$ (km s^{-1})	2.8 ± 0.5
[Fe/H]	0.08 ± 0.07
[Na/H]	0.18 ± 0.06
[Mg/H]	0.20 ± 0.05
[Si/H]	0.24 ± 0.05
[Ca/H]	0.18 ± 0.13
[Sc/H]	0.09 ± 0.11
[Ti/H]	0.12 ± 0.06
[V/H]	0.16 ± 0.11
[Cr/H]	0.10 ± 0.04
[Co/H]	0.14 ± 0.06
[Ni/H]	0.15 ± 0.05
log A(Li)	<0.96 ± 0.10
Distance	330 ± 50 pc
Parameters from MCMC analysis.	
P (d)	4.378 090 ± 0.000 006
$T_{\rm c}$ (HJD) (UTC)	245 5921.6527 ± 0.0005
T_{14} (d)	0.2225 ± 0.0017
$T_{12} = T_{34}$ (d)	$0.017^{+0.002}_{-0.001}$
$\Delta F = R_{\rm P}^2/R_*^2$	0.006 09 ± 0.000 17
b	$0.26^{+0.13}_{-0.15}$
i (°)	87.8 ± 1.3
K_1 (km s^{-1})	0.039 ± 0.003
γ (km s^{-1})	−23.712 ± 0.003
e	0 (adopted) (<0.22 at 3σ)
M_* ($M_\odot$)	1.32 ± 0.05
R_* ($R_\odot$)	$1.88^{+0.10}_{-0.06}$
log g_* (CGS)	$4.01^{+0.02}_{-0.04}$
ρ_* ($\rho_\odot$)	$0.198^{+0.017}_{-0.025}$
$T_{\rm eff}$ (K)	5570 ± 90
$M_{\rm P}$ ($M_{\rm Jup}$)	0.38 ± 0.03
$R_{\rm P}$ ($R_{\rm Jup}$)	$1.43^{+0.10}_{-0.06}$
log $g_{\rm P}$ (CGS)	2.62 ± 0.05
$\rho_{\rm P}$ ($\rho_{\rm J}$)	0.13 ± 0.02
$\rho_{\rm P}$ (CGS)	0.17 ± 0.03
a (au)	0.0574 ± 0.0007
$T_{\rm P,A\,=0}$ (K)	1540 ± 40

Errors are 1σ; Limb-darkening coefficients were (Euler r) a1 = 0.679, a2 = −0.433, a3 = 1.017 and a4 = −0.494; (Trapp Iz) a1 = 0.766, a2 = −0.688, a3 = 1.056 and a4 = −0.479.

of transiting planetary systems (mass <3 $M_\odot$). The rms scatter of the calibrating sample around the best fit is 0.027 dex for log(mass) and 0.009 dex for log(radius).

For each system we list the resulting parameters in Tables 2–8, and plot the resulting data and models in Figs 1–7. We also refer the reader to Smith et al. (2012) who present an extensive analysis of the effect of red noise in the transit light curves on the resulting system parameters.

As in the past WASP papers we plot the spectroscopic $T_{\rm eff}$, and the stellar density from fitting the transit, against the evolutionary tracks from Girardi et al. (2000), as shown in Fig. 8. Note that, in the analyses presented here, the comparisons with the evolutionary models are not fed back into the system modelling.

Table 7. System parameters for WASP-66.

1SWASP J103254.00−345923.3	
2MASS 10325399−3459234	
TYCHO-2 7193-1804-1	
RA = $10^h32^m54\overset{s}{.}00$, Dec. = $-34^\circ59'23\overset{''}{.}3$ (J2000)	
V mag = 11.6	
Rotational modulation	<1 mmag
pm (RA) 11.0 ± 0.8 (Dec.) -13.1 ± 0.8 mas yr^{-1}	
Stellar parameters from spectroscopic analysis.	
Spectral type	F4
$T_{\rm eff}$ (K)	6600 ± 150
$\log g$	4.3 ± 0.2
$\xi_{\rm t}$ (km s^{-1})	2.2 ± 0.3
$v \sin I$ (km s^{-1})	13.4 ± 0.9
[Fe/H]	-0.31 ± 0.10
[Na/H]	-0.29 ± 0.06
[Mg/H]	-0.27 ± 0.10
[Si/H]	-0.19 ± 0.06
[Ca/H]	-0.19 ± 0.10
[Sc/H]	-0.17 ± 0.12
[Ti/H]	-0.16 ± 0.15
[V/H]	-0.10 ± 0.11
[Cr/H]	-0.25 ± 0.15
[Mn/H]	-0.37 ± 0.12
[Co/H]	-0.15 ± 0.08
[Ni/H]	-0.38 ± 0.10
$\log A$(Li)[LTE]	3.06 ± 0.11
$\log A$(Li)[N-LTE]	2.97 ± 0.11
Distance	380 ± 100 pc
Parameters from MCMC analysis.	
P (d)	$4.086\,052 \pm 0.000\,007$
$T_{\rm c}$ (HJD) (UTC)	$245\,5929.096\,15 \pm 0.000\,35$
T_{14} (d)	0.1876 ± 0.0017
$T_{12} = T_{34}$ (d)	0.018 ± 0.002
$\Delta F = R_{\rm P}^2/R_*^2$	0.00668 ± 0.00016
b	$0.48^{+0.06}_{-0.08}$
i (°)	85.9 ± 0.9
K_1 (km s^{-1})	0.246 ± 0.011
γ (km s^{-1})	-10.02458 ± 0.00013
e	0 (adopted) (<0.11 at 3σ)
M_* ($M_\odot$)	1.30 ± 0.07
R_* ($R_\odot$)	1.75 ± 0.09
$\log g_*$ (CGS)	4.06 ± 0.04
ρ_* ($\rho_\odot$)	$0.242^{+0.036}_{-0.028}$
$T_{\rm eff}$ (K)	6580 ± 170
$M_{\rm P}$ ($M_{\rm Jup}$)	2.32 ± 0.13
$R_{\rm P}$ ($R_{\rm Jup}$)	1.39 ± 0.09
$\log g_{\rm P}$ (CGS)	3.44 ± 0.05
$\rho_{\rm P}$ ($\rho_{\rm J}$)	$0.860^{+0.17}_{-0.13}$
$\rho_{\rm P}$ (CGS)	$1.14^{+0.22}_{-0.17}$
a (au)	0.0546 ± 0.0009
$T_{\rm P,A\,=0}$ (K)	1790 ± 60

Errors are 1σ; Limb-darkening coefficients were (Euler r) a1 = 0.353, a2 = 0.759, a3 = −0.628 and a4 = 0.177; (Trapp Iz) a1 = 0.443, a2 = 0.299, a3 = −0.213 and a4 = 0.022.

Table 8. System parameters for WASP-67.

1SWASP J194258.51−195658.4	
2MASS 19425852−1956585	
TYCHO-2 6307-1388-1	
RA = $19^h42^m58\overset{s}{.}51$, Dec. = $-19^\circ56'58\overset{''}{.}4$ (J2000)	
V mag = 12.5	
Rotational modulation	<3 mmag
pm (RA) 0.7 ± 1.3 (Dec.) -33.8 ± 2.4 mas yr^{-1}	
Stellar parameters from spectroscopic analysis.	
Spectral type	K0V
$T_{\rm eff}$ (K)	5200 ± 100
$\log g$	4.35 ± 0.15
$\xi_{\rm t}$ (km s^{-1})	0.9 ± 0.1
$v \sin I$ (km s^{-1})	2.1 ± 0.4
[Fe/H]	-0.07 ± 0.09
[Na/H]	0.11 ± 0.08
[Mg/H]	0.05 ± 0.04
[Si/H]	0.15 ± 0.03
[Ca/H]	0.02 ± 0.12
[Ti/H]	0.01 ± 0.06
[V/H]	0.09 ± 0.08
[Cr/H]	0.06 ± 0.03
[Co/H]	0.05 ± 0.04
[Ni/H]	0.00 ± 0.08
$\log A$(Li)	$<0.23 \pm 0.11$
Distance	225 ± 45 pc
Parameters from MCMC analysis.	
P (d)	$4.614\,42 \pm 0.000\,01$
$T_{\rm c}$ (HJD) (UTC)	$245\,5824.3742 \pm 0.0002$
T_{14} (d)	0.079 ± 0.001
$\Delta F = R_{\rm P}^2/R_*^2$	$0.0181^{+0.0013}_{-0.0005}$
b	$0.94^{+0.05}_{-0.03}$
i (°)	$85.8^{+0.3}_{-0.4}$
K_1 (km s^{-1})	0.056 ± 0.004
γ (km s^{-1})	-0.5634 ± 0.0002
e	0 (adopted) (<0.20 at 3σ)
M_* ($M_\odot$)	0.87 ± 0.04
R_* ($R_\odot$)	0.87 ± 0.04
$\log g_*$ (CGS)	4.50 ± 0.03
ρ_* ($\rho_\odot$)	1.32 ± 0.15
$T_{\rm eff}$ (K)	5240 ± 10
$M_{\rm P}$ ($M_{\rm Jup}$)	0.42 ± 0.04
$R_{\rm P}$ ($R_{\rm Jup}$)	$1.4^{+0.3}_{-0.2}$
$\log g_{\rm P}$ (CGS)	$2.7^{+0.1}_{-0.2}$
$\rho_{\rm P}$ ($\rho_{\rm J}$)	0.16 ± 0.08
$\rho_{\rm P}$ (CGS)	0.21 ± 0.10
a (au)	0.0517 ± 0.0008
$T_{\rm P,A\,=0}$ (K)	1040 ± 30

Errors are 1σ; Limb-darkening coefficients were (Euler r) a1 = 0.671, a2 = −0.540, a3 = 1.225 and a4 = −0.574; (Trapp Iz) a1 = 0.744, a2 = −0.707, a3 = 1.134 and a4 = −0.506.

5 WASP-47

WASP-47 is a G9 star ($V = 11.9$) with a possibly elevated metallicity of [Fe/H] = 0.18 ± 0.07. There is no significant detection of lithium in the spectra, with an equivalent width upper limit of 3 mÅ, corresponding to an abundance upper limit of $\log A(\mathrm{Li}) < 0.81 \pm 0.10$. The temperature of 5400 K along with the lithium abundance implies a lower age limit of around 0.6 Gyr when compared with the Hyades cluster (Sestito & Randlich 2005). The rotation rate ($P = 15 \pm 3$ d) implied by the $v \sin I$ (assuming that the planet's orbit is aligned, and thus that the star's spin axis is perpendicular to us) gives a gyrochronological age of $\sim 1.0^{+0.7}_{-0.4}$ Gyr using the Barnes (2007) relation.

With an orbital period of 4.16 d, a mass of 1.14 $M_{\rm Jup}$ and a radius of 1.15 $R_{\rm Jup}$, WASP-47b is an entirely typical hot Jupiter.

6 WASP-55

WASP-55 is a G1 star ($V = 11.8$) with a below-solar metallicity of [Fe/H] = −0.20 ± 0.07. The lithium abundance in WASP-55

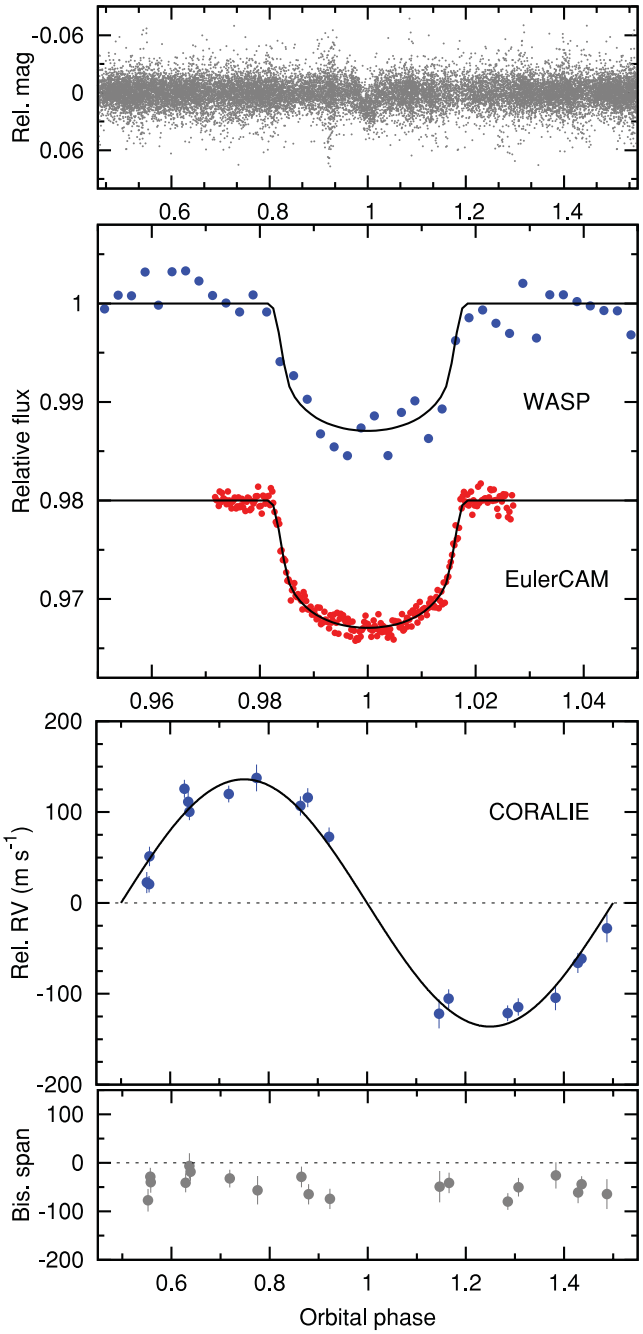

Figure 1. WASP-47b discovery data. Top panel: the WASP-South light curve folded on the transit period. Second panel: the binned WASP data with (offset) the follow-up transit light curves (ordered from the top as in Table 1) together with the fitted MCMC model. Third panel: the CORALIE radial velocities with the fitted model. Bottom panel: the bisector spans; the absence of any correlation with radial velocity is a check against transit mimics.

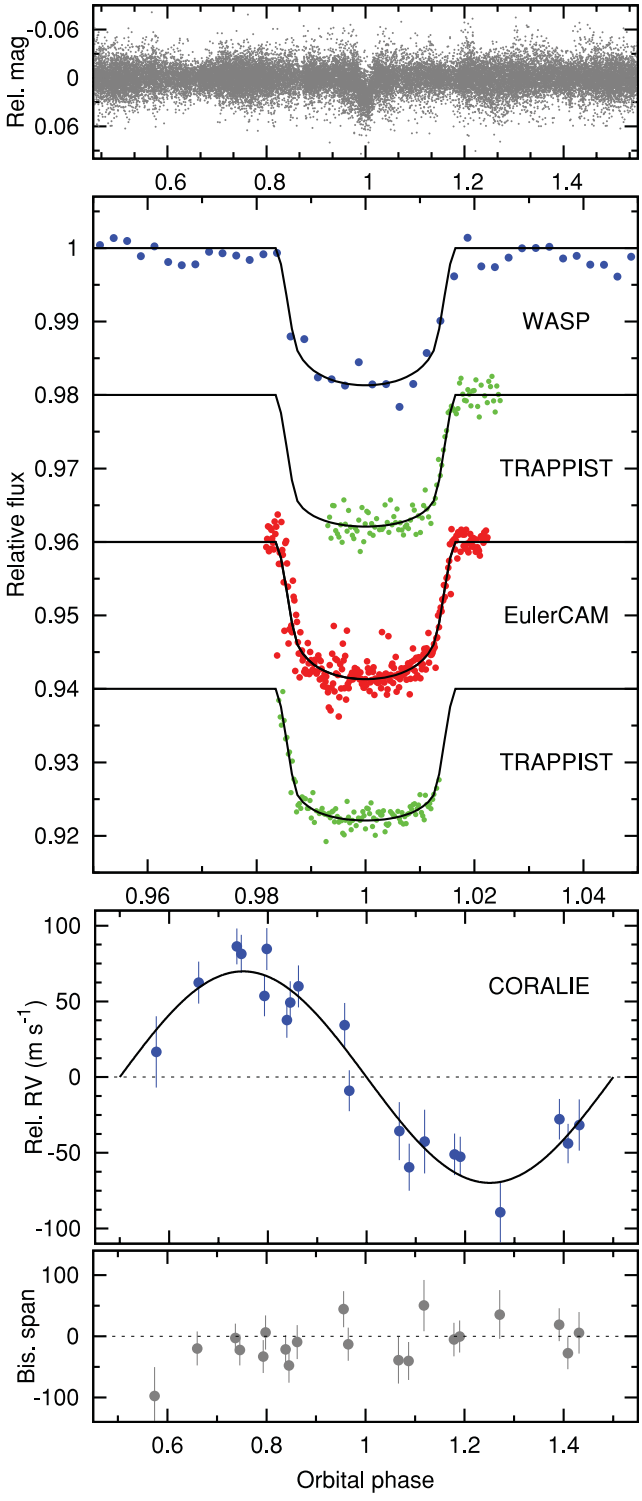

Figure 2. WASP-55b discovery data (as in Fig. 1).

implies an age of $\gtrsim$2 Gyr (Sestito & Randlich 2005). The rotation rate ($P = 20 \pm 7$ d) implied by the $v \sin I$ gives a gyrochronological age of $\sim 3^{+5}_{-2}$ Gyr using the Barnes (2007) relation.

Two Micron All Sky Survey (2MASS) images of WASP-55 show a star approximately 2 arcsec away and about 5 mag fainter. This is sufficiently faint that it is unlikely to be affecting our results significantly.

WASP-55b is moderately inflated, with a mass of 0.57 $M_{\rm Jup}$ and a radius of 1.30 $R_{\rm Jup}$, though this is in line with many known hot Jupiters.

7 WASP-61

WASP-61 is an F7 star ($V = 12.5$) with metallicity near solar (the poor quality of our spectrum prevents more detailed analysis than

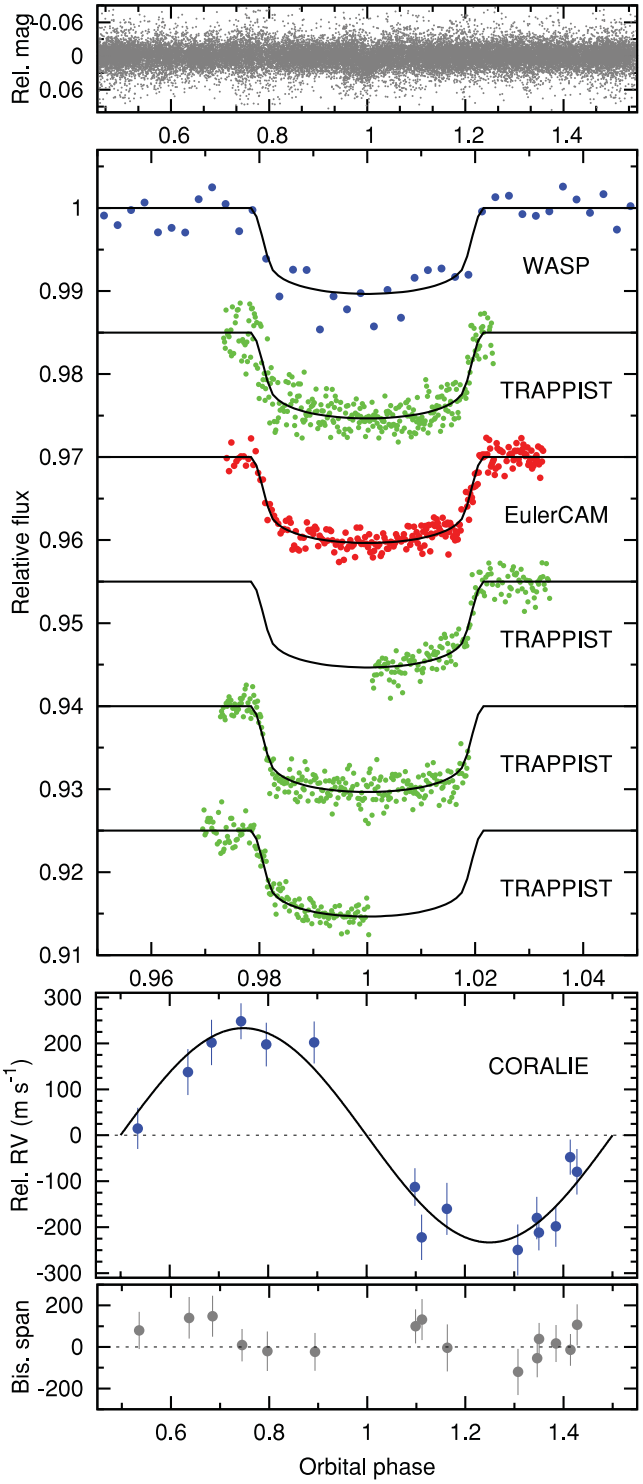

Figure 3. WASP-61b discovery data (as in Fig. 1).

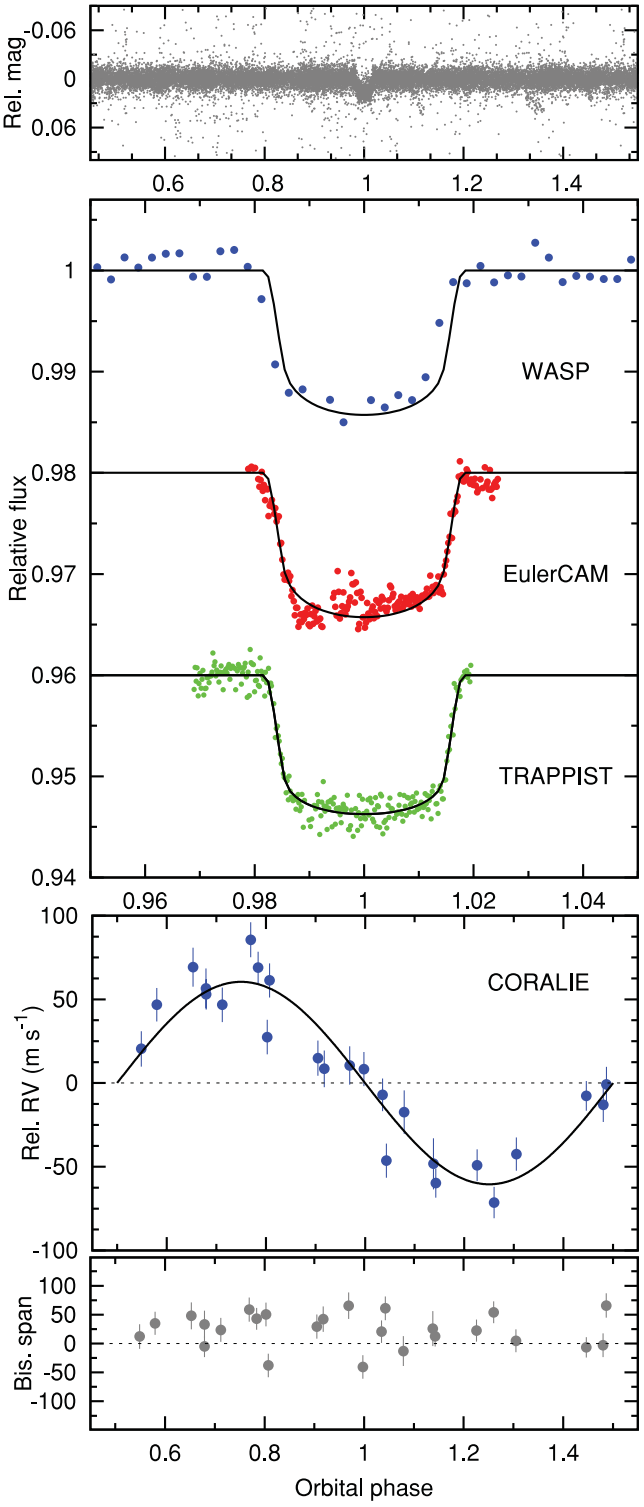

Figure 4. WASP-62b discovery data (as in Fig. 1).

the [Fe/H] $= -0.10 \pm 0.12$ reported in Table 4). There is no significant detection of lithium in the spectra, corresponding to an abundance upper limit of $\log A(\mathrm{Li}) < 1.1 \pm 0.1$, which implies an age of several Gyr (Sestito & Randlich 2005). The rotation rate ($P = 6.3 \pm 0.9$ d) implied by the $v \sin I$ gives a gyrochronological age of $\sim 0.7^{+1.2}_{-0.4}$ Gyr using the Barnes (2007) relation.

WASP-61b has a high mass of $M = 2.1\,M_{\rm Jup}$ and the highest density of the planets reported here, at $\rho = 1.1\,\rho_{\rm Jup}$ (1.4 g cm^{-3}).

8 WASP-62

WASP-62 is an F7 star ($V = 10.3$) with a solar metallicity. For a star of this temperature (6230 ± 80 K), the presence of relatively strong lithium absorption in the spectrum does not provide a strong age constraint; this level of depletion is found in clusters as young as $\sim$0.5 Gyr (Sestito & Randlich 2005). The rotation rate ($P = 6.3 \pm 0.8$ d) implied by the $v \sin I$ gives a gyrochronological age

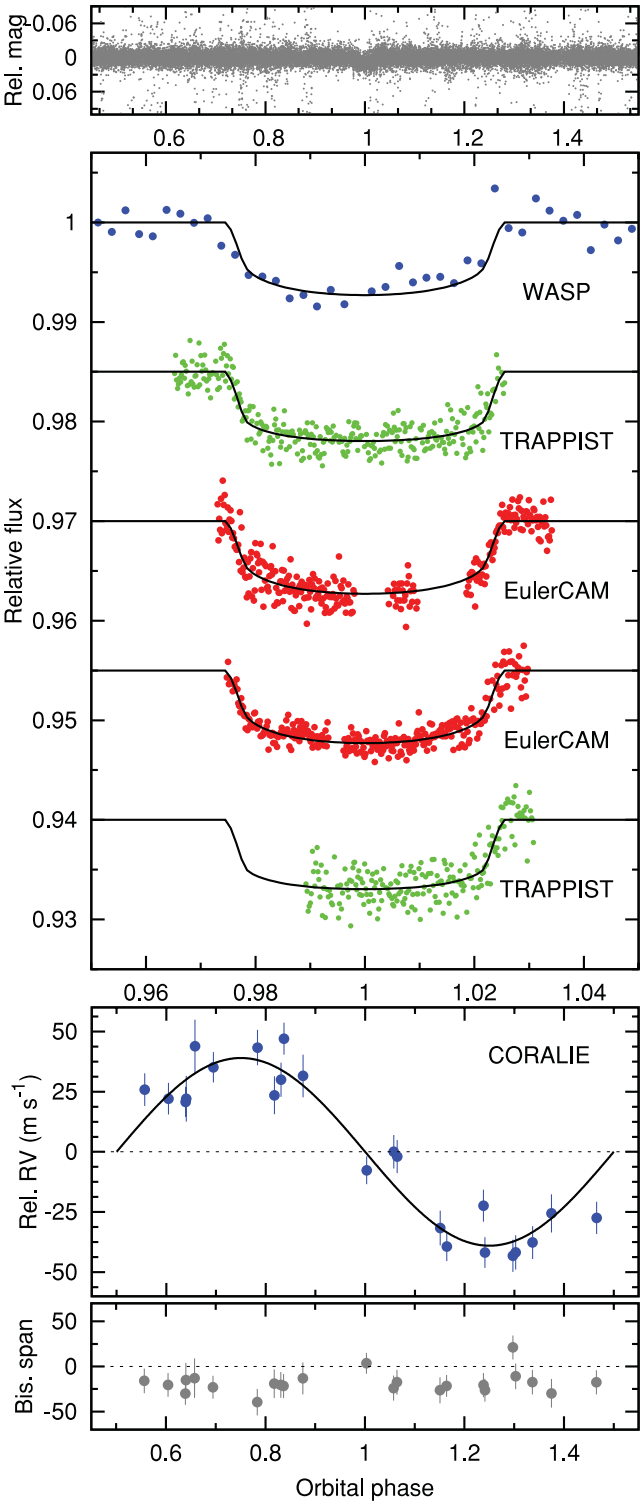

Figure 5. WASP-63b discovery data (as in Fig. 1).

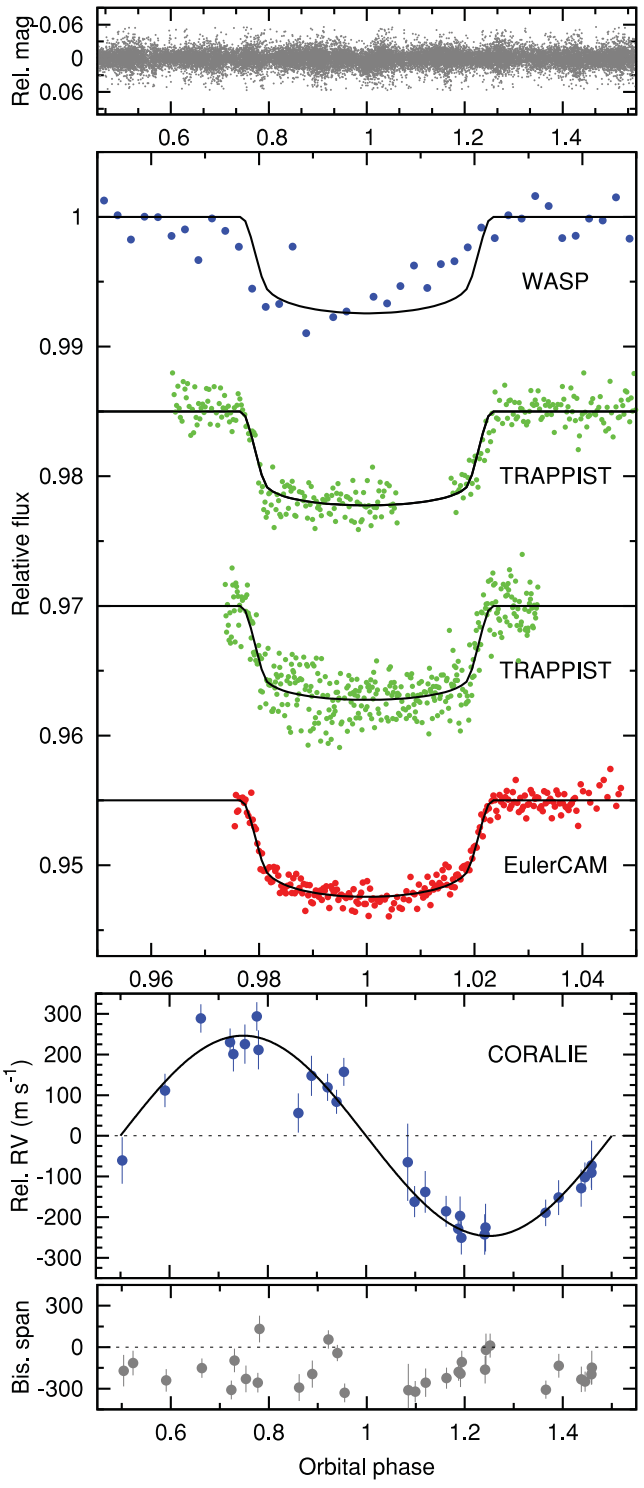

Figure 6. WASP-66b discovery data (as in Fig. 1); the two parts of the upper TRAPPIST curve were taken on different nights.

of $\sim 0.7^{+0.4}_{-0.3}$ Gyr using the Barnes (2007) relation. There are no emission peaks evident in the Ca II H&K lines.

The EulerCAM transit light curve is badly affected by weather. Our MCMC analysis balances χ^2 across the different data sets, so inflates the error bars of this light curve. We also ran the analysis omitting this curve, which led to results that were the same within the errors.

9 WASP-63

WASP-63 is a G8 star ($V = 11.2$) with solar metallicity. There is no significant detection of lithium in the spectra, with an equivalent width upper limit of 11 mÅ, corresponding to an abundance upper limit of $\log A(\mathrm{Li}) < 0.96 \pm 0.10$. This implies an age of at least several Gyr (Sestito & Randlich 2005). The rotation rate ($P = 37 \pm 9$ d) implied by the $v \sin I$ gives a gyrochronological age of

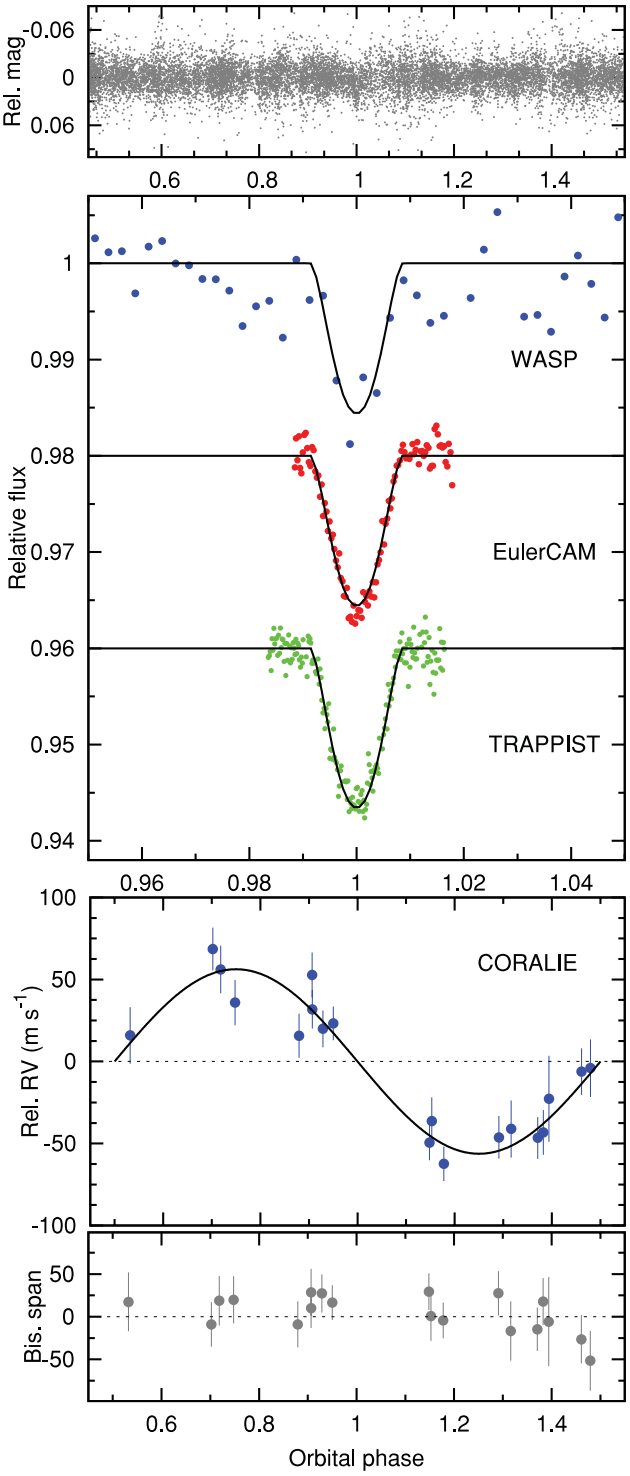

Figure 7. WASP-67b discovery data (as in Fig. 1).

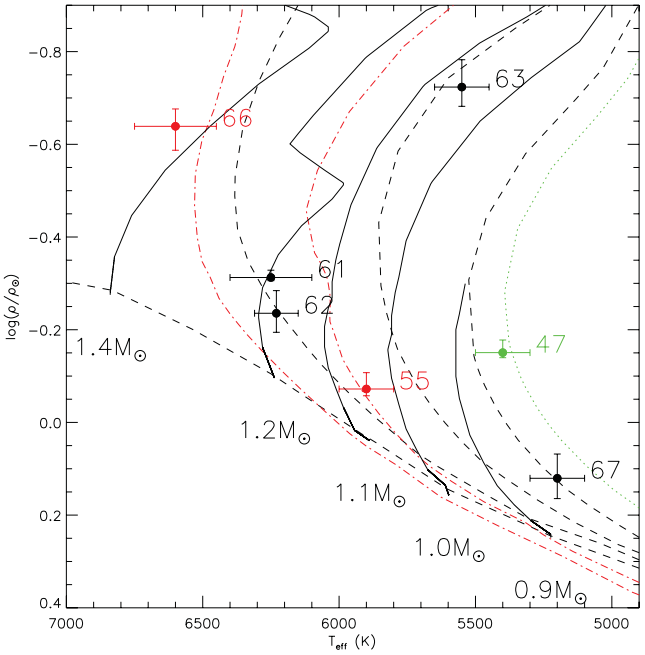

Figure 8. Evolutionary tracks on a modified H–R diagram ($\rho_*^{-1/3}$ versus $T_{\rm eff}$). The black lines are for solar metallicity, [Fe/H] = 0, showing (solid lines) mass tracks with the labelled masses and (dashed lines) age tracks for log (age) = 7.8, 9.4, 9.9 and 10.2 yr. The four host stars with near-solar metallicities are shown in black. The green-labelled WASP-47 has above-solar metallicity of [Fe/H] = +0.18, and the green dotted line is the age track for [Fe/H] = +0.18 and log (age) = 10.2 yr. The red dot–dashed lines are for a below-solar metallicity of [Fe/H] = −0.2, being at ages log (age) = 9.4 and 9.8 yr. The two host stars with below-solar metallicities are labelled in red. The data are from Girardi et al. (2000).

$\sim 6^{+5}_{-3}$ Gyr using the Barnes (2007) relation. There are no emission peaks evident in the Ca II H&K lines.

The stellar radius is inflated for a G8 star and indicates that WASP-63 has evolved off the main sequence (see Fig. 8), with an age of ∼8 Gyr.

The planet WASP-63b is the least massive of those reported here, at 0.38 $M_{\rm Jup}$, and also has the lowest density ($\rho = 0.13\,\rho_{\rm Jup}$ or 0.17 g cm^{-3}). This indicates that mechanisms causing inflated planet radii need to be able to operate late on in the evolution of a planetary system.

10 WASP-66

WASP-66 is an F4 star ($V = 11.6$) with a below-solar metallicity of [Fe/H] = −0.31 ± 0.10. With $T_{\rm eff} = 6600 \pm 150$ K WASP-66 is relatively hot among known hot-Jupiter hosts. The presence of strong lithium absorption in the spectrum suggests that WASP-66 is $\lesssim$2 Gyr old (Sestito & Randlich 2005). The rotation rate ($P = 4.9 \pm 1.3$ d) implied by the $v \sin I$ gives little age constraint, $3.3^{+10}_{-2.7}$ Gyr, from the Barnes (2007) relation.

With a mass of 2.3 $M_{\rm Jup}$ WASP-66b is the most massive of the planets reported here.

11 WASP-67

WASP-67 is an K0V star ($V = 12.5$) with a solar metallicity. There is no significant detection of lithium in the spectra, with an equivalent width upper limit of 5 mÅ, corresponding to an abundance upper limit of $\log A({\rm Li}) < 0.23 \pm 0.11$. This implies an age of at least ∼0.5 Gyr (Sestito & Randlich 2005). The rotation rate ($P = 25 \pm 7$ d) implied by the $v \sin I$ gives a gyrochronological age of $2.0^{+1.6}_{-1.0}$ Gyr using the Barnes (2007) relation. There are no emission peaks evident in the Ca II H&K lines.

WASP-67b has a mass of 0.42 $M_{\rm Jup}$ and a radius of 1.4 $R_{\rm Jup}$, making it inflated ($\rho = 0.16\,\rho_{\rm Jup}$). It also has a high impact factor of $b = 0.94$, making the transit curve V shaped. If the criterion $X = b + R_{\rm P}/R_* > 1$ is satisfied then the transit is grazing, with

part of the planet not transiting the stellar face (see e.g. Smalley et al. 2011). For WASP-67b this value is $1.07^{+0.05}_{-0.03}$, and, further, out of 375 000 MCMC steps only 17 had $X < 1$. This implies a $>3\sigma$ probability that the transit is grazing, making WASP-67b the first hot Jupiter known to have a grazing transit, following WASP-34 and HAT-P-27/WASP-40 that are possibly grazing (Anderson et al. 2011; Smalley et al. 2011).

The fact that some of the planet's disc does not transit the star makes the fitted planet radius highly correlated with the impact parameter, b. The planet radius is still constrained by the transit depth, coupled with the timings of first and fourth contact, and the fact that the stellar radius is also constrained. The star is constrained by the transit and the spectroscopic temperature and metallicity, coupled with the Southworth (2011) calibration, and the resulting mass and radius are consistent with a K0V star (see e.g. Fig. 8).

Nevertheless, the loss of second and third contact in a grazing system reduces the information constraining the model and for this reason the error bars on the planet radius are much bigger (≈20 per cent) than for the other systems we present (≈4–7 per cent).

12 DISCUSSION

It has often been noted that the hot-Jupiter population shows an apparent 'pile-up' at orbital periods of $P = 3$–4 d. We can use the increasing numbers of hot Jupiters, primarily from the ground-based transit surveys, to investigate this. In the following we discuss the relative period distribution of hot Jupiters, but do not consider their absolute occurrence rate (for which see e.g. Wright et al. 2012).

As a first step we take the sample of confirmed planets compiled by Schneider et al. (2011), as of 2012 March, limiting this to periods less than 8 d and planetary masses of 0.1–12 $M_{\rm Jup}$ (the super-Earths may well be a different population dynamically). We show (Fig. 9) the cumulative distributions against orbital period, semimajor axis and Roche limit separation. These confirm that we see more planets at periods of $P \approx 3$–5 d, with fewer at shorter and longer periods. However, this compilation comes from many different surveys, each of which will have different selection effects, and so needs to be interpreted with caution.

We thus create a second sample of planets discovered by the transit surveys ($P < 8$ d, $M = 0.1$–$12\,M_{\rm Jup}$), based on the Schneider et al. compilation but with unpublished WASP planets added up to WASP-84b. This sample of 163 planets is dominated by WASP (81 planets), HAT (34), *Kepler* (18) and *CoRoT* (14).

The inclination range that produces a transit scales with semi-major axis as $\cos^{-1}(R_*/a)$. To compare this with the distribution of orbital periods, which are securely known, we can translate this to P by assuming a star of solar mass and radius. Further, the biggest factor affecting discovery probability in a WASP-like survey is the number of transits recorded, which will scale as P^{-1}. In Fig. 10 we show the distribution of WASP-South candidates, which indicates that a P^{-1} function, though imperfect, is a rough approximation.

We caution that this is only a very preliminary account of relevant selection effects, which will be different for each of the above surveys. For example, the number of transits required is likely to saturate above some number (this number depending on the survey and the amount of data), and WASP-like surveys at only one longitude will also suffer from sampling effects at integer-day periods.

Nevertheless, we can multiply together the transit probability and the P^{-1} function to produce a detection-probability curve (dotted red curve in Fig. 11), and we can use this to produce a 'corrected' planet distribution curve.

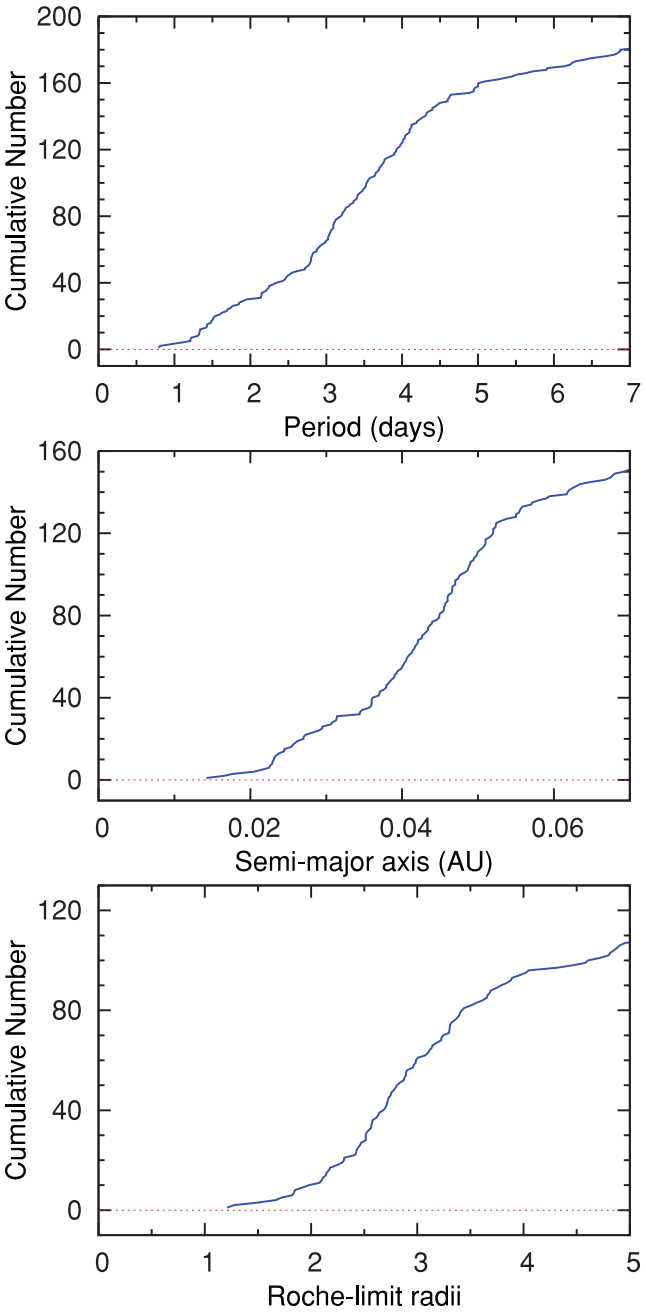

Figure 9. The cumulative distributions of (top) orbital period, (middle) semimajor axis and (bottom) separations in units of Roche limit separation for a sample of hot Jupiters (see text). The definition of Roche limit separation is taken from Ford & Rasio (2006).

One can interpret this curve as showing four regions with different slopes, the slopes having relative ratios (for corrected number of planets versus period interval) of 1 : 10 : 40 : 12. The need for different slopes in the different regions is significant on a Kolmogorov–Smirnov (KS) test at >95 per cent probabilities. We caution, though, that we regard this as an indicative description of the distribution, rather than a unique one, and the relative slopes are of course dependent on the uncertain selection effects.

The four regions of the hot-Jupiter period distribution are as follows.

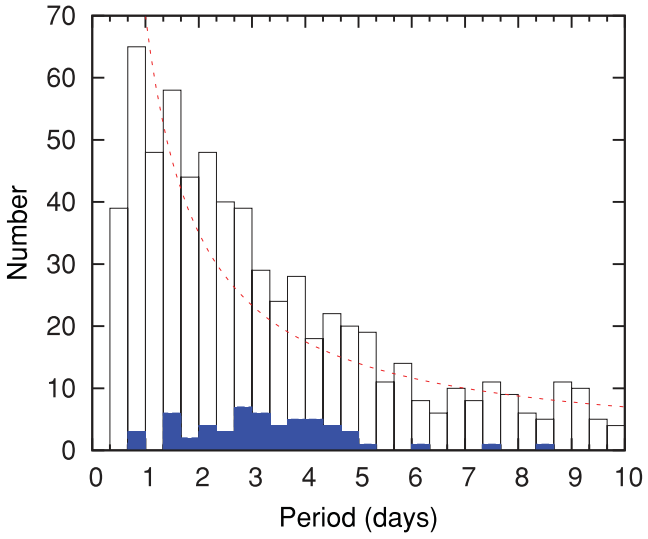

Figure 10. The open histogram shows the period distribution of all WASP-South candidates that have been rejected or confirmed as planets. The solid histogram shows the planets. The dotted line is a simple P^{-1} function, scaling as the number of transits observed in a WASP-like survey.

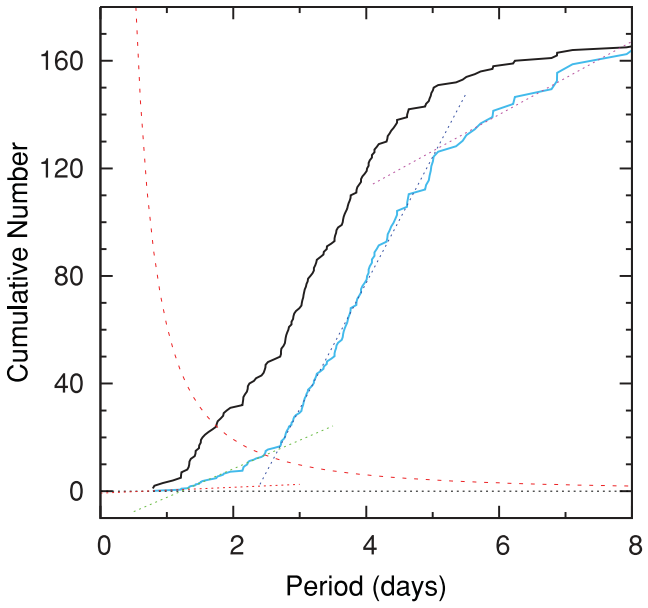

Figure 11. The solid black line is the cumulative distribution of orbital periods for transiting hot Jupiters. The solid blue line is the same but corrected for the probability of detection (which is the dotted curve). The dotted straight lines are a suggested parametrization of the distribution (see text).

(1) $P = 0.8$–1.2 d, containing only four planets (WASP-19b, WASP-43b, WASP-18b and WASP-12b; Hebb et al. 2009, 2010; Hellier et al. 2009, 2011b), despite the probability of detection being greatest. These planets are thought to be tidally decaying on relatively short time-scales, and so are rare, found only by the surveys sampling the most stars (see the discussion in Hellier et al. 2011b; note that WASP observes from one longitude with greater sky coverage than HATnet, whereas HATnet covers less sky but from several longitudes).

There are no known hot Jupiters with a period below the $P = 0.79$-d of WASP-19b. Despite the fact that the probability of detection of such planets in WASP data is at its highest (see Fig. 11, curve), the number of good candidates declines (Fig. 10), and, further, we have followed up over 40 such candidates without success (compared to an overall success rate of 1 in 12). Thus hot-Jupiter planets below $P = 0.79$-d must be very rare (there are several super-Earths with such periods, though their tidal-decay rate will of course be much lower).

(2) $P = 1.2$–2.7 d. The abundance is an order of magnitude greater than in the 0.8–1.2 d range, but still a factor of $\sim$4 lower than in the range of 2.7–5 d.

(3) $P = 2.7$–5 d. Our analysis confirms the existence of a pile-up of hot Jupiters, and suggests that it has a relatively well defined lower edge at $P = 2.7$ d.

Ford & Rasio (2006) argued that a hot-Jupiter population resulting from circularization of highly eccentric orbits will have an inner edge at two Roche limit radii ($2a_{\rm R}$), where $a_{\rm R} = \frac{R_{\rm P}}{0.462}\left(\frac{M_{\rm P}}{M_*}\right)^{1/3}$.

For a planet of Jupiter mass and radius around a star of solar mass and radius, $2\,a_{\rm R}$ corresponds to $P = 1.2$ d, and so would explain our finding of a break at that period. The few systems inside that limit are presumably spiralling inwards relatively rapidly under tidal decay (e.g. Matsumura, Peale & Rasio 2010).

Further, for an inflated planet with a radius of $R \approx 1.8\,R_{\rm Jup}$ (as seen in the highly inflated planets WASP-12b, WASP-17b, WASP-78b, WASP-79b, HAT-P-32b and HAT-P-33b; Hebb et al. 2009; Anderson et al. 2010; Hartman et al. 2011; Smalley et al. 2012) $2\,a_{\rm R}$ equates to $P = 2.7$ d (again assuming a $1\,M_{\rm Jup}$ planet orbiting a Sun-like star). Hence, if hot Jupiters arrive in the pile-up with a range of radius inflations, the Ford & Rasio argument would produce a cut-off ranging from $\sim$1.2 to 2.7 d, which might explain our finding of breaks at both those values.

(4) $P = \gtrsim 5$ d. The upper edge of the pile-up appears to be near 5 d, although we caution that in WASP-like surveys the detection probability (and hence number of planets) decreases, and the selection effects get worse, as the period increases beyond $P \sim 5$ d.

In addition to the smaller number of transits at longer periods, the ground-based transit surveys are heavily biased towards inflated planets (which produce deeper transits). As the period lengthens and the stellar irradiation reduces it is likely that fewer planets are inflated (Demory & Seager 2011), which would reduce the numbers found by WASP-like surveys.

The period distribution of hot Jupiters is likely to result from several physical mechanisms. These include disc migration and possible 'stopping mechanisms' (e.g. Matsumura, Pudritz & Thommes 2007), third-body interactions, such as the Kozai mechanism, that can move planets on to highly eccentric orbits that are then tidally captured and circularize at short periods (e.g. Guillochon, Ramirez-Ruiz & Lin 2011; Naoz et al. 2011), and orbital decay and in-spiral caused by tidal interactions with the host star (e.g. Matsumura et al. 2010).

Study of the angle between the planetary orbit and the stellar rotation axis indicates that many current orbits are likely to result from the Kozai mechanism (e.g. Triaud et al. 2010), but it is probable that the hot Jupiters are a composite population with differing past histories. Thus, to further investigate the pile-up, we need to accumulate statistics to look for differences in, for example, the orbital eccentricities and the spin–orbit angle between the different period ranges that we have outlined.

ACKNOWLEDGMENTS

WASP-South is hosted by the South African Astronomical Observatory and we are grateful for their ongoing support and assistance.

Funding for WASP comes from consortium universities and from the UK's Science and Technology Facilities Council. TRAPPIST is funded by the Belgian Fund for Scientific Research (Fond National de la Recherche Scientifique, FNRS) under the grant FRFC 2.5.594.09.F, with the participation of the Swiss National Science Fundation (SNF). MG and EJ are FNRS Research Associates.

REFERENCES

Anderson D. R. et al., 2010, ApJ, 709, 159
Anderson D. R. et al., 2011, PASP, 123, 555
Anderson D. R. et al., 2012, MNRAS, 422, 1988
Bakos G. À., Noyes R. W., Kovács G., Stanek K. Z., Sasselov D. D., Domsa I., 2004, PASP, 116, 266
Barnes S. A., 2007, ApJ, 669, 1167
Batalha N. M. et al., 2012, ApJS, preprint (arXiv:1202.5852)
Bruntt H. et al., 2010, MNRAS, 405, 1907
Claret A., 2000, A&A, 363, 1081
Collier Cameron A. et al., 2007a, MNRAS, 375, 951
Collier Cameron A. et al., 2007b, MNRAS, 380, 1230
Demory B.-O., Seager S., 2011, ApJS, 197, 12
Enoch B., Collier Cameron A., Parley N. R., Hebb L., 2010, A&A, 516, A33
Ford E. B., Rasio F. A., 2006, ApJ, 638, L45
Gillon M. et al., 2009, A&A, 496, 259
Girardi L., Bressan A., Bertelli G., Chiosi C., 2000, A&AS, 141, 371
Guillochon J., Ramirez-Ruiz E., Lin D. N. C., 2011, ApJ, 732, 74
Hartman J. D. et al., 2011, ApJ, 742, 59
Hebb L. et al., 2009, ApJ, 693, 1920
Hebb L. et al., 2010, ApJ, 708, 224
Hellier C. et al., 2009, Nat, 460, 1098
Hellier C. et al., 2011a, in Bouchy F., Díaz R., Moutou C., eds, Detection and Dynamics of Transiting Exoplanets (EPJ Web Conf., 11, 01004)
Hellier C. et al., 2011b, A&A, 535, L7
Jehin E. et al., 2011, Messenger, 145, 2
Magain P., 1984, A&A, 134, 189
Matsumura S., Pudritz R. E., Thommes E. W., 2007, ApJ, 660, 1609
Matsumura S., Peale S. J., Rasio F. A., 2010, ApJ, 725, 1995
Maxted P. F. L. et al., 2011, PASP, 123, 547
Naoz S., Farr W. M., Lithwick Y., Rasio F. A., Teyssandier J., 2011, Nat, 473, 187
Navarro J. F., Abadi M. G., Venn K. A., Freeman K. C., Anguiano B., 2011, MNRAS, 412, 1203
Pollacco D. et al., 2006, PASP, 118, 1407
Pollacco D. et al., 2008, MNRAS, 385, 1576
Schneider J., Dedieu C., Le Sidaner P., Savalle R., Zolotukhin I., 2011, A&A, 532, A79
Sestito P., Randlich S., 2005, A&A, 442, 615
Smalley B. et al., 2011, A&A, 526, 130
Smalley B. et al., 2012, A&A, preprint (arXiv:1206.1177)
Smith A. M. S. et al., 2012, AJ, 143, 81
Southworth J., 2011, MNRAS, 417, 2166
Triaud A. H. M. J. et al., 2010, A&A, 524, 25
Wright J. T., Marcy G. W., Howard A. W., Johnson J. A., Morton T., Fischer D. A., 2012, ApJ, 753, 160
Zacharias N. et al., 2010, AJ, 139, 2184

SUPPORTING INFORMATION

Additional Supporting Information may be found in the online version of this article:

Table A1. CORALIE radial velocities.

Please note: Wiley-Blackwell are not responsible for the content or functionality of any supporting materials supplied by the authors. Any queries (other than missing material) should be directed to the corresponding author for the article.

This paper has been typeset from a TEX/LATEX file prepared by the author.